Supplementary Materials

for “Thermodynamic Advantage of Transient Wave Dynamics in Hierarchical Decision Architectures”

Oleg Dolgikh • Draft v1 • 2026-01-29

Working draft. Sections and numbering may shift in revision; all metrics/definitions are stable.

Contents

Supplementary Methods

S1. Mathematical specification of CRN

CRN (Coherent Resonant Netting) is defined as a two-stage decision architecture. Stage-I performs a low-amplitude, wave-like exploration that prunes a hypothesis space at low marginal cost, and Stage-II corresponds to a high-gain commitment/readout mechanism (e.g., spiking fixation) that acts on the pruned set. In this Supplementary Materials we formalize Stage-I as an open-system wave proxy and evaluate its functional outputs via absorption into Target vs Distractor sinks.

S1.1 Graph and state space

Let G=(V,E) be a directed graph with $|V|=N$ nodes and weighted edges $w_{ij}\geq 0$. Stage-I dynamics are represented by a density matrix $\rho(t)$ on an N-dimensional state space $\{|i\rangle\}$. The diagonal $\rho_{ii}(t)$ is interpreted as node occupancy probability (population proxy).

Baseline Hamiltonian from a symmetrized weighted Laplacian:

$$H0 = -\gamma \cdot L_{sym}, \quad \text{where} \quad L_{sym} = D_{sym} - W_{sym}, \quad W_{sym} = (W + W^{T})/2.$$

S1.2 Open-system dynamics (GKSL proxy)

Stage-I is modeled with the GKSL master equation with dephasing and absorbing sinks. GKSL is used as a functional proxy for transient wave dynamics with tunable decoherence/measurement, not as a claim of microscopic quantum coherence in neural tissue.

$$d\rho/dt = -i\,[H, \rho] + \kappa \cdot \Sigma_k \left(|k\rangle\langle k|\,\rho\,|k\rangle\langle k| - \tfrac{1}{2}\{|k\rangle\langle k|, \rho\}\right) + \Sigma_{s\in S}\,\eta_s \cdot \left(J_s\,\rho\,J_s^{\dagger} - \tfrac{1}{2}\{J_s^{\dagger} J_s, \rho\}\right).$$

κ controls the coherence–measurement balance (κ→0: coherent exploration; $\kappa \gg 1$: Zeno-like classicalization). Sinks are implemented by jump operators J_s that remove population from designated nodes into external accumulators (Target vs Distractor).

S1.3 Disorder parameter ε

Energetic heterogeneity is modeled as diagonal disorder:

$$H = H0 + \mathrm{diag}(E), \quad \text{with} \quad E_i \sim \mathrm{Uniform}[-\varepsilon, +\varepsilon].$$

S1.4 Metrics

At T_end we report sink absorption probabilities P_T (Target) and P_D (Distractor), and define:

$$\mathrm{Selectivity\_end} = P_T / (P_D + \delta), \quad \mathrm{coverage\_end} = P_T + P_D.$$

$$\mathrm{Utility}(\lambda) = P_T - \lambda \cdot P_D, \quad \mathrm{InfoPerCost} = \mathrm{Utility}(\lambda) / (\mathrm{coverage\_end} + \chi).$$

$$P_{good} = \Pr(\mathrm{Selectivity\_end} > \theta \mid P_T > pT_{min}).$$

Unless stated otherwise: $\lambda=1$, $\chi=0.01$, $\theta=2.0$, $pT_{min}=0.005$.

S2. Datasets and graph construction

S2.1 C. elegans touch circuit

A small C. elegans subcircuit (touch → interneurons → motor outputs) derived from Varshney et al. is used as a minimal connectome benchmark. Nodes are grouped into sensory sources, target motor outputs, and distractor outputs. The task is formulated as absorption into target vs distractor sinks.

S2.2 Drosophila larva mushroom body (Winding et al. 2023)

A directed weighted graph is built from the larval Drosophila connectome (Winding et al., Science 2023). We extract an MB-centered subgraph and an active subgraph connecting selected PN sources to MBON sinks.

Table S1. Drosophila graph sizes used in Bridge-A.

Graph	nodes	edges
core MB subgraph	379	2137
extended MB subgraph	553	3875
active subgraph (core)	80	381
active subgraph (extended)	243	1765

Extended-graph benchmark selection sizes: PN sources=10, MBON targets=5, MBON distractors=5.

S2.3 Mouse cortical proxy (SBM)

A stochastic block model with hierarchical feed-forward structure is used as a mouse cortical proxy to probe scalability and the permeability–selectivity trade-off.

S3. Simulation protocol and default parameters

Unless stated otherwise we use γ=1.0, η_sink=1.0, dt=0.05, T_end=10.0. Each condition is evaluated over multiple disorder draws and, where applicable, multiple surrogate graphs.

Table S2. Key numerical parameters (Drosophila benchmark config).

parameter	value
gamma	1.0
eta_sink	1.0
dt	0.05
T_max/T_end	10.0
kappa_grid	0.001, 0.003, 0.01, 0.03, 0.1, 0.3, 1.0, 3.0, 10.0

S4. Baselines and negative controls

Baselines include a classical random walk (CRW) and a thermal random walk in the same energy landscape at $T_{env} \in \{0.1, 1.0\}$. Negative controls include degree-preserving rewiring within edge types and partial lesions of KC→MBON projections.

S5. Statistical analysis

We report two-way ANOVA for main effects of architecture variant and disorder ε on Selectivity_end and coverage_end, and bootstrap confidence intervals for the DES effect Δ(ε=3−ε=0) within each architecture. Between-architecture comparisons bootstrap the difference in DES magnitudes.

Supplementary Results

S6. Universal DES across scales (conceptual figures)

These figures are used in the main text to anchor the Two-Factor Mechanism and the cross-scale DES claim.

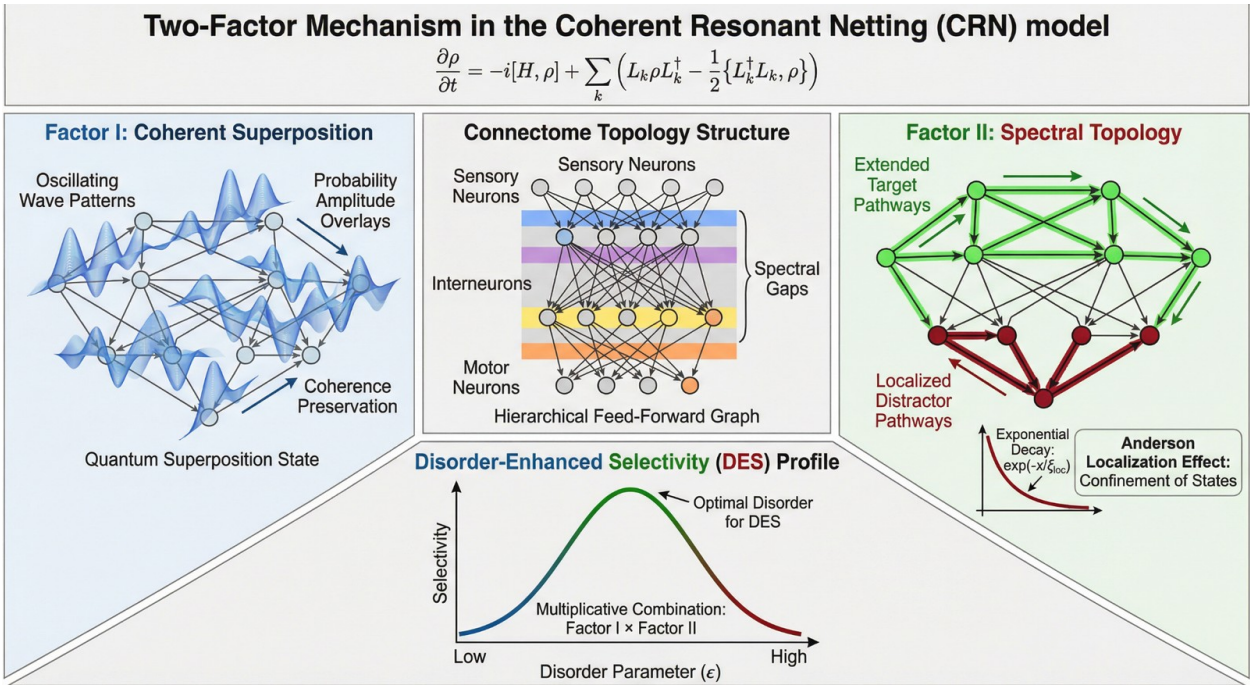

Supplementary Figure S1. Two-Factor Mechanism schematic (Factor I: coherence proxy; Factor II: spectral topology).

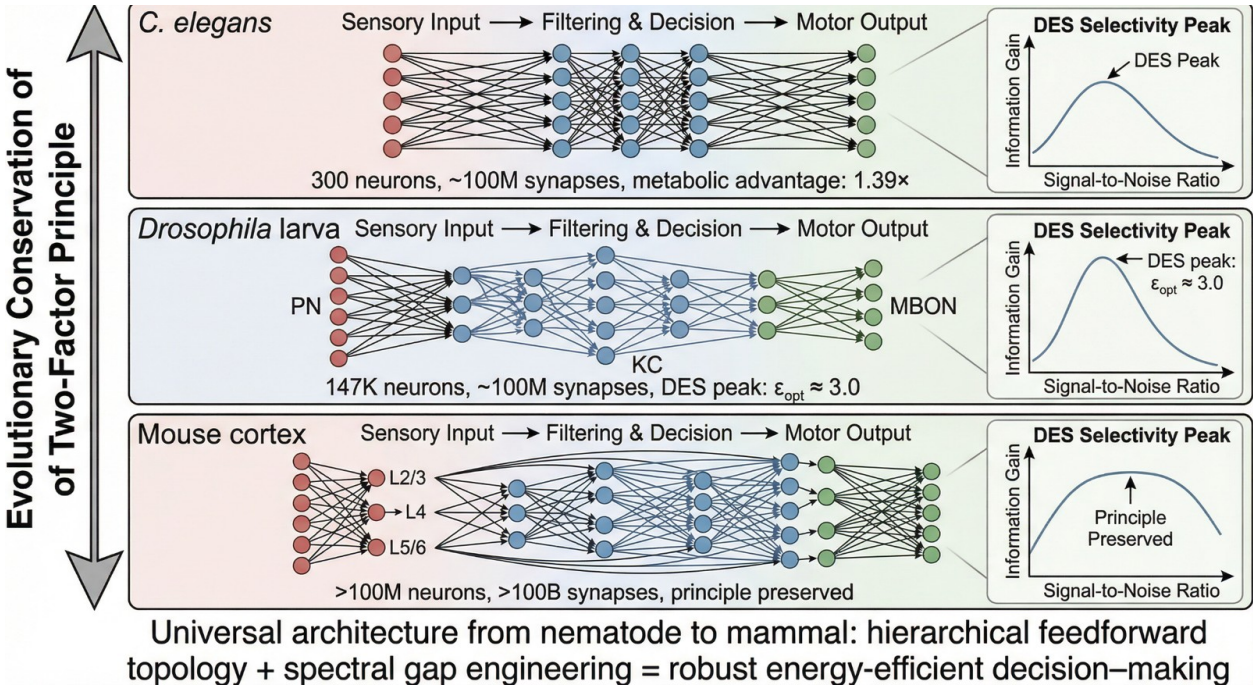

Supplementary Figure S2. Universal hierarchical decision architecture schematic across scales (nematode → insect → mammal).

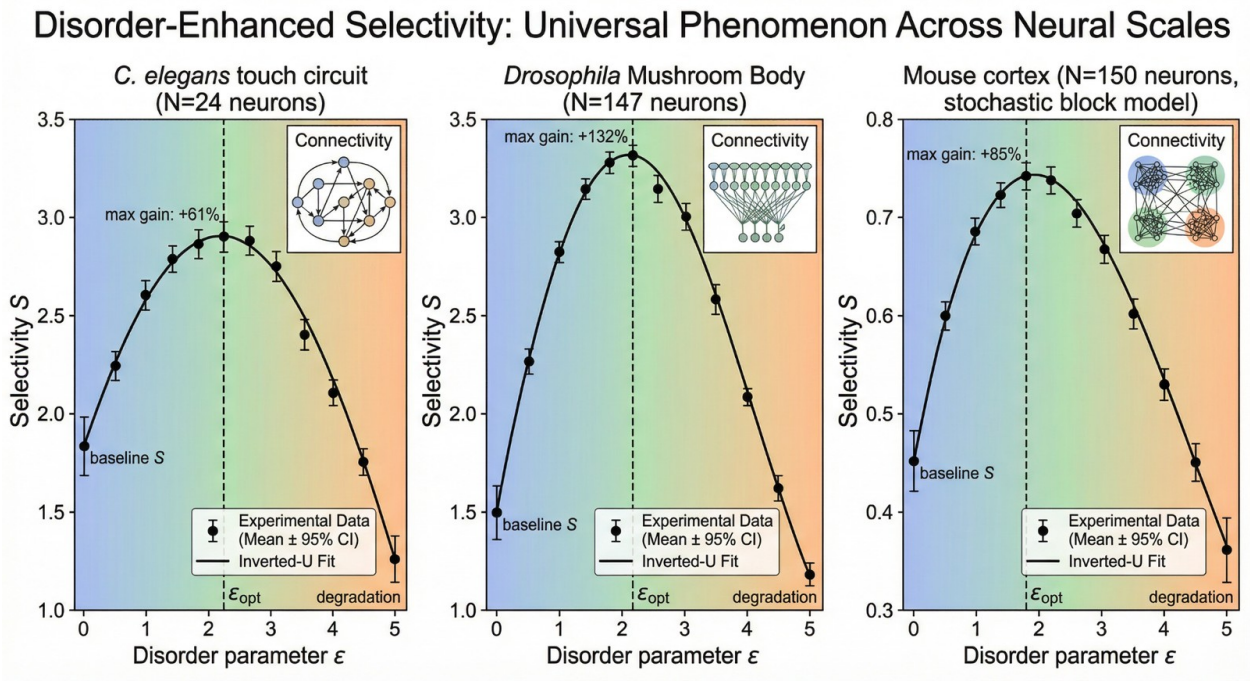

Supplementary Figure S3. Disorder-Enhanced Selectivity (DES) across three substrates (C. elegans, Drosophila, mouse proxy).

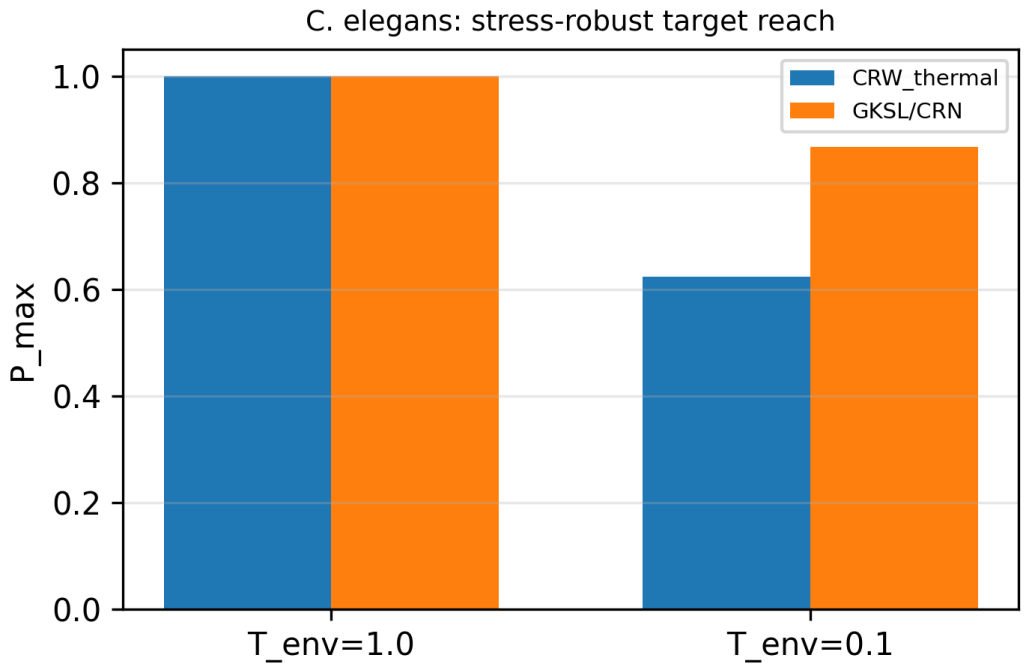

Supplementary Figure S4. C. elegans touch circuit: maximum target absorption P_max at T_env=1.0 and T_env=0.1 for the wave proxy vs thermal baseline.

S7. Drosophila larva connectome benchmark (A7)

Table S3 summarizes best-by-objective GKSL performance as a function of disorder ε, alongside CRW and thermal baselines. Note: for ε=5, the best-by-selectivity metric is undefined under the minimum-throughput filter used in the sweep.

Table S3. A7 compact summary (Drosophila benchmark).

eps	k_sel	Sel_GKSL	cov_GKSL	PT_GKSL	PD_GKSL	k_IPC	IPC_GKSL	Sel_CRW	IPC_CRW	Sel_T0.1	IPC_T0.1	Sel_T1.0	IPC_T1.0
0	1	1.52	0.0122	0.007357	0.00484	1	0.1134	0.8783	-0.06352	0.8783	-0.06352	0.8783	-0.06352
1	1	1.558	0.009416	0.005736	0.00368	1	0.1058	0.8783	-0.06352	0.9071	-0.04691	0.9752	-0.01223
2	0.3	1.544	0.008445	0.005125	0.00332	1	0.1064	0.8783	-0.06352	1.274	0.1157	0.9368	-0.03187
3	0.001	2.224	0.007904	0.005452	0.002452	0.001	0.1676	0.8783	-0.06352	1.252	0.1066	1.037	0.01762
5						1	0.06066	0.8783	-0.06352	1.167	0.07357	0.983	-0.008244

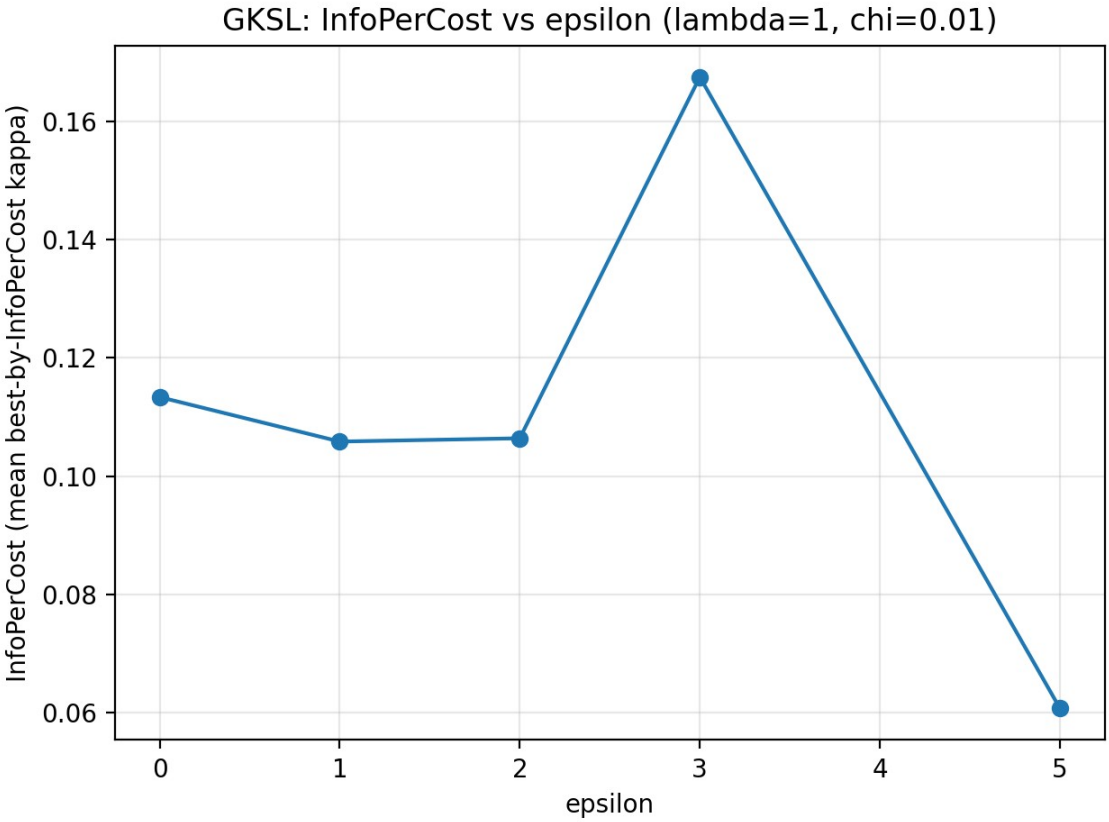

Supplementary Figure S5. Best-by-InfoPerCost across disorder ε (A7).

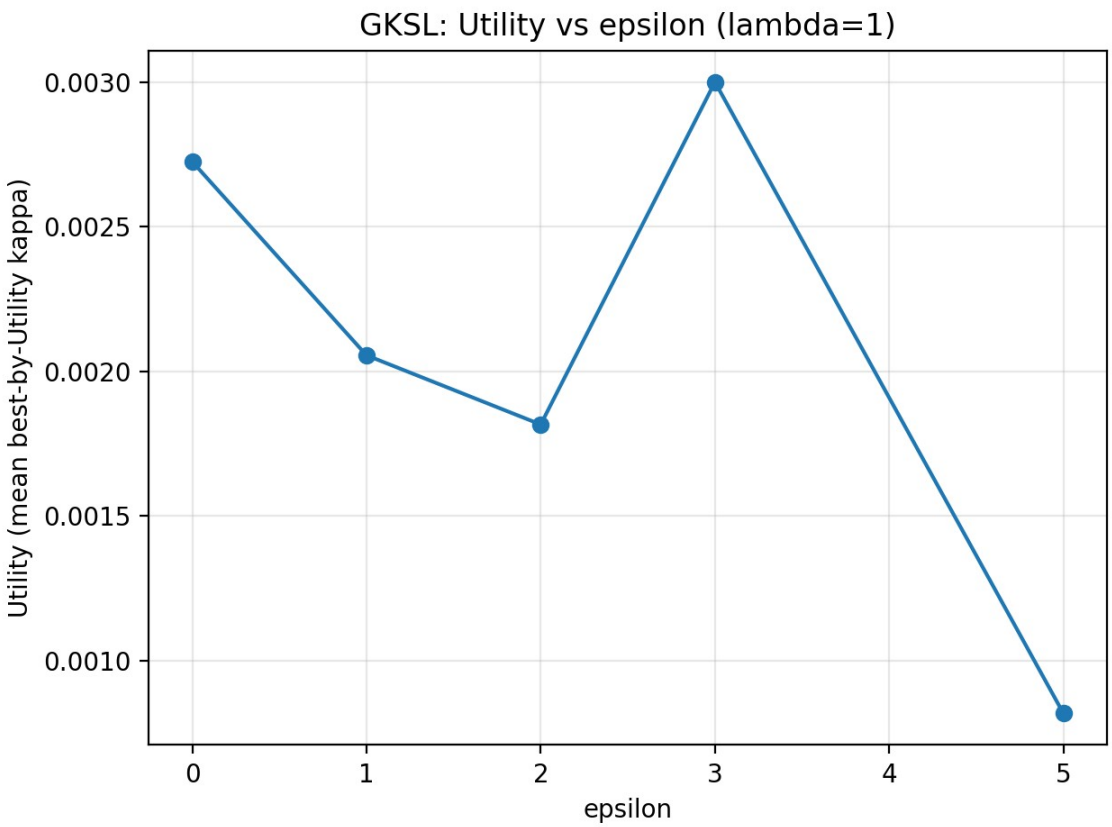

Supplementary Figure S6. Best-by-Utility across disorder ε (A7).

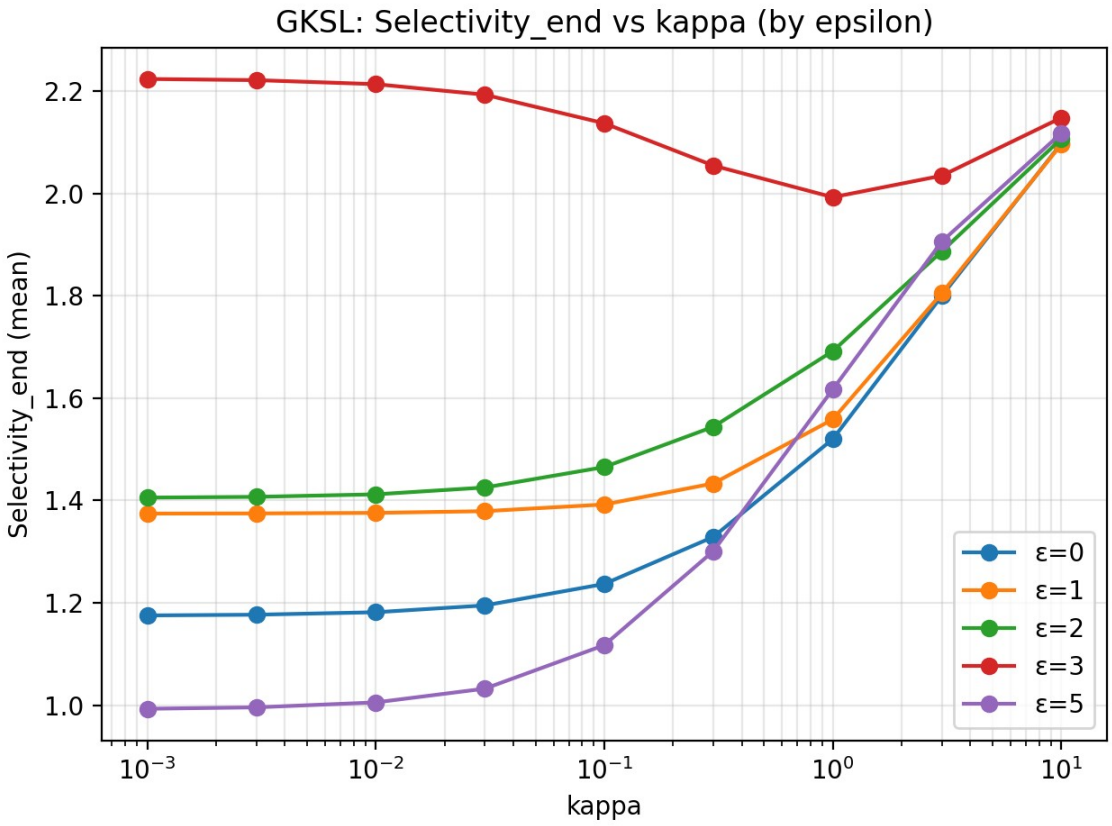

Supplementary Figure S7. Selectivity_end vs κ for multiple ε (A7).

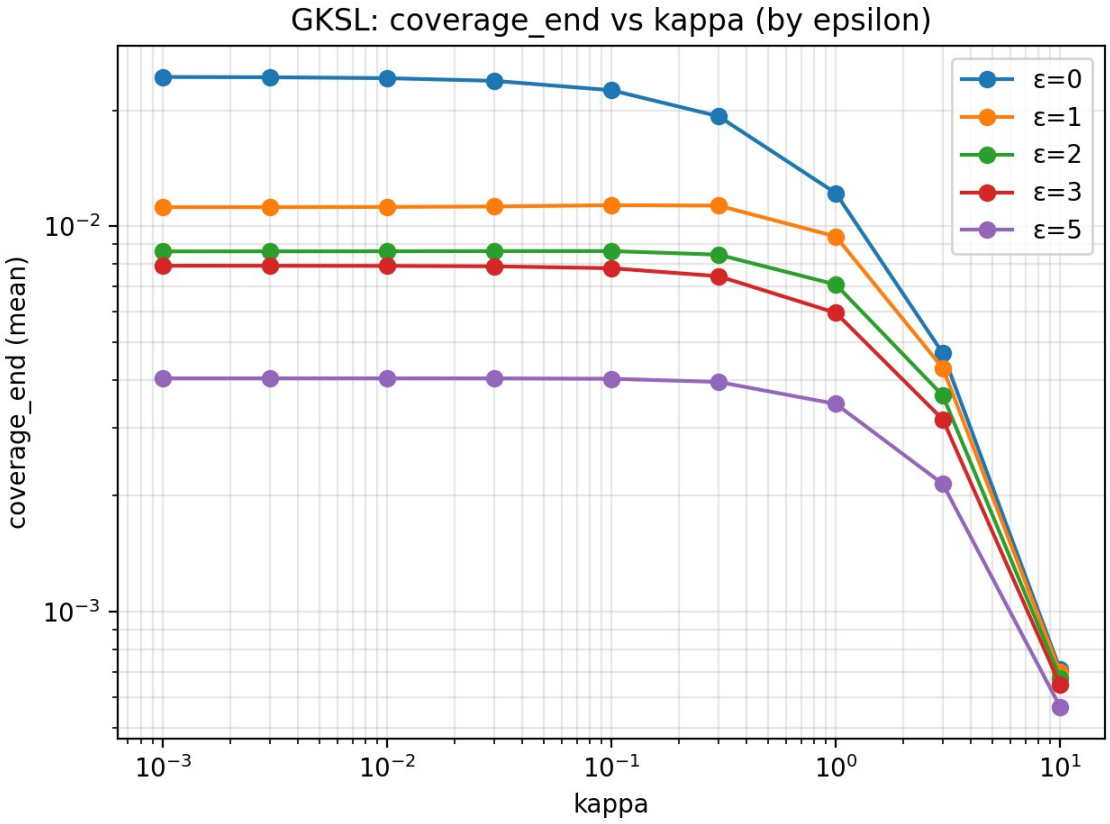

Supplementary Figure S8. coverage_end vs κ for multiple ε (A7).

S8. Localization diagnostics (A8.4)

We report participation-ratio diagnostics and differential localization ΔPR = PR_target − PR_distractor.

Table S4. Localization diagnostics by ε (κ=0.001).

epsilon	n_trials	Selectivity_end_mean	Selectivity_end_std	delta_PR_mean	delta_PR_std	ratio_PR_mean	ratio_PR_std
0	10	1.175	0	-1.961	2.341e-16	0.6072	0
1	10	1.408	0.3943	-0.7682	1.175	0.7978	0.3145
2	10	1.687	0.8646	-0.1843	0.5956	0.9599	0.1628
3	10	3.524	4.945	-0.09162	1.232	1.054	0.4415
5	10	1.361	1.249	0.05169	1.045	1.082	0.4161

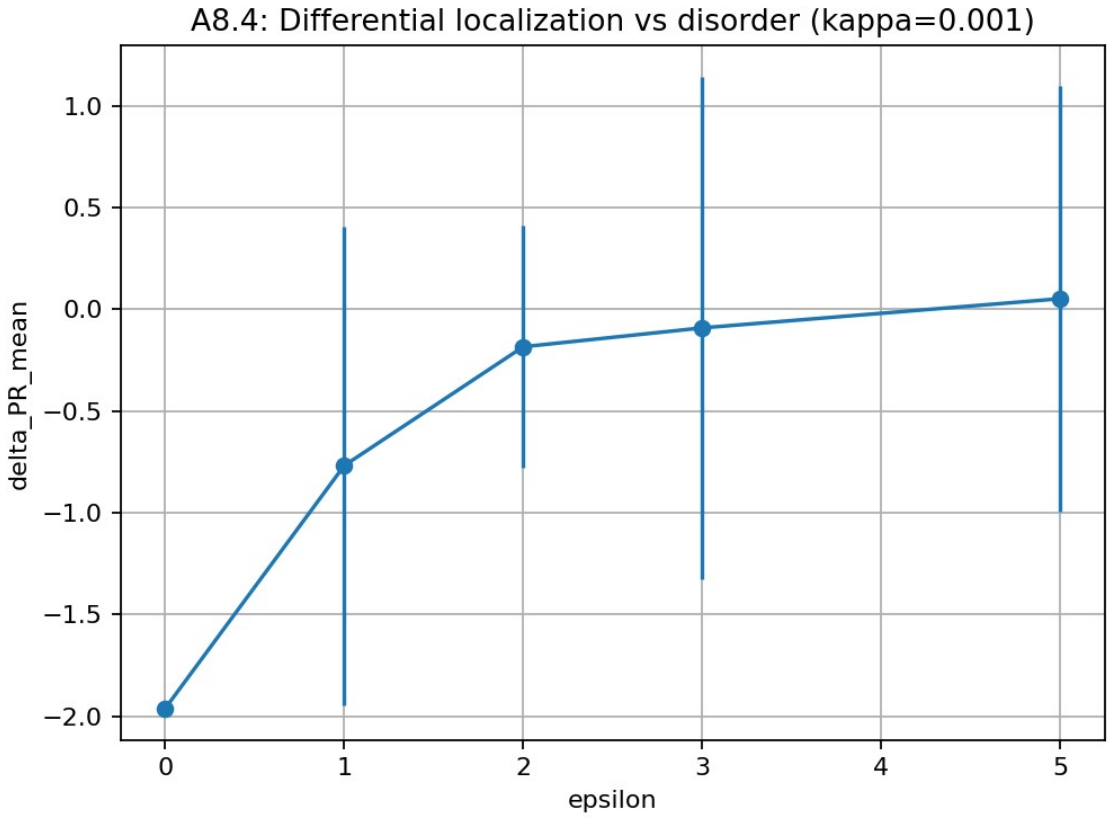

Supplementary Figure S9. ΔPR vs ε at κ=0.001 (A8.4).

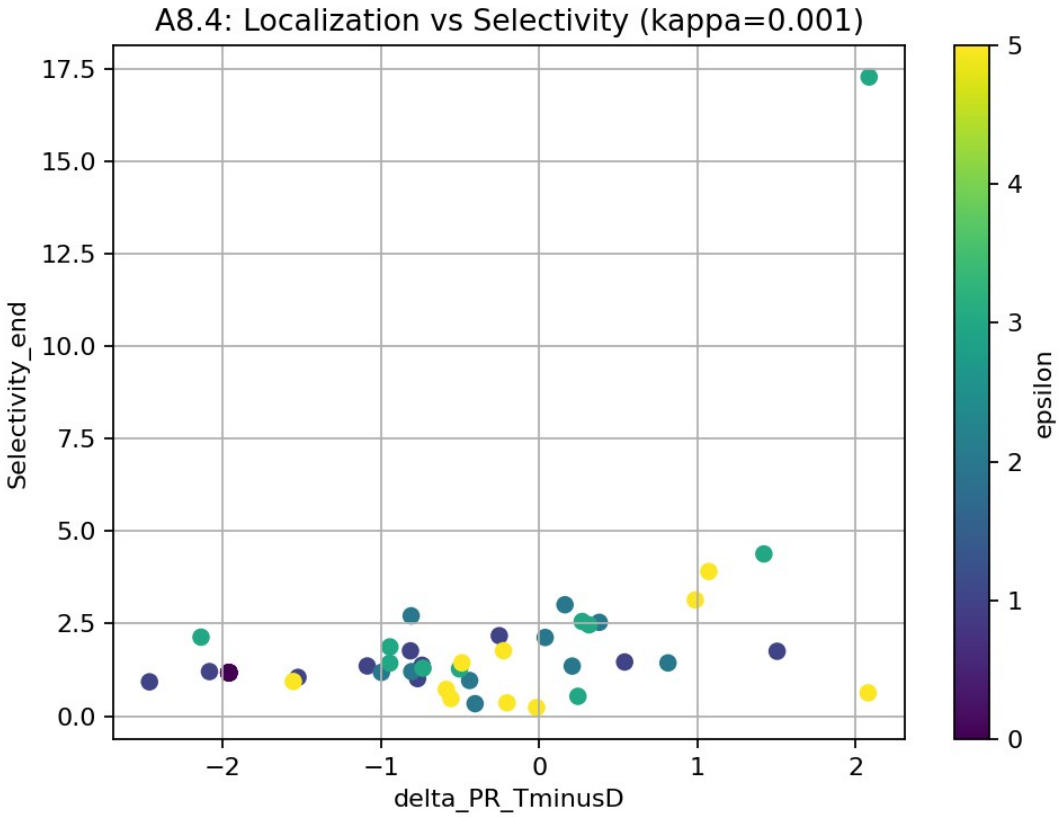

Supplementary Figure S10. Selectivity_end vs ΔPR scatter (A8.4).

S9. Architecture dependence and negative controls (A8.5–A8.6)

Two-way ANOVA and bootstrap tests quantify architecture × disorder effects and the DES peak dependency on topology.

Table S5. Two-way ANOVA (κ=0.001).

Metric	Effect	F	df1	df2	p_value
Selectivity_end	VARIANT	44.7	2	4097	6.25e-20
Selectivity_end	EPSILON	31.12	4	4095	1.45e-25
Selectivity_end	ALL_CELLS	20.53	14	4085	4.16e-51
coverage_end	VARIANT	14.33	2	4097	6.28e-07
coverage_end	EPSILON	2907	4	4095	<1e-300
coverage_end	ALL_CELLS	932.4	14	4085	<1e-300

Table S6. Bootstrap DES within variants (κ=0.001).

variant	contrast	delta	CI_low	CI_high	significance
lesion_KC_MBON	DES = Selectivity_end(ε=3) - Selectivity_end(ε=	1.102	0.83	1.398	significant

	0)				
lesion_KC_MBON	Selectivity_end(ε=3) - Selectivity_end(ε=5)	-0.502	-0.832	-0.188	significant
original	DES = Selectivity_end(ε=3) - Selectivity_end(ε=0)	1.489	0.249	3.355	significant
original	Selectivity_end(ε=3) - Selectivity_end(ε=5)	-0.898	-2.805	0.491	ns
rewired_type	DES = Selectivity_end(ε=3) - Selectivity_end(ε=0)	0.162	0.056	0.274	significant
rewired_type	Selectivity_end(ε=3) - Selectivity_end(ε=5)	0.436	0.21	0.672	significant

Table S7. Bootstrap DES between variants (κ=0.001).

contrast	delta	CI_low	CI_high	significance
DES(original) - DES(rewired_type)	1.328	0.069	3.232	p<0.001
DES(original) - DES(lesion_KC_MBON)	0.383	-0.902	2.261	ns
DES(lesion_KC_MBON) - DES(rewired_type)	0.938	0.646	1.254	p<0.001

Table S8. Architecture dependence metrics (κ=0.001).

variant	epsilon	n_runs_total	mean_P_sink_T_end	mean_P_sink_D_end	Selectivity_end_mean	Selectivity_ratioOfMeans	coverage_end_mean
lesion_KC_MBON	0	400	0.01647	0.01396	1.194	1.18	0.03042
lesion_KC_MBON	1	400	0.009295	0.007022	1.454	1.324	0.01632
lesion_KC_MBON	2	400	0.007125	0.004964	1.702	1.435	0.01209
lesion_KC_MBON	3	400	0.006401	0.003987	2.296	1.605	0.01039
lesion_KC_MBON	5	400	0.002816	0.002368	1.795	1.189	0.005184
original	0	20	0.01319	0.01122	1.175	1.175	0.02441
original	1	20	0.006436	0.005012	1.362	1.284	0.01145
original	2	20	0.00472	0.003596	1.569	1.312	0.008316
original	3	20	0.004564	0.002589	2.662	1.763	0.007153
original	5	20	0.002089	0.00156	1.762	1.339	0.003649
rewired_type	0	400	0.0126	0.01254	1.062	1.005	0.02515
rewired_type	1	400	0.008359	0.008874	1.113	0.9419	0.01723
rewired_type	2	400	0.006022	0.006077	1.255	0.991	0.0121
rewired_typ	3	400	0.004412	0.004895	1.225	0.9014	0.009307

e							
rewired_type	5	400	0.002553	0.002638	1.659	0.9681	0.005191

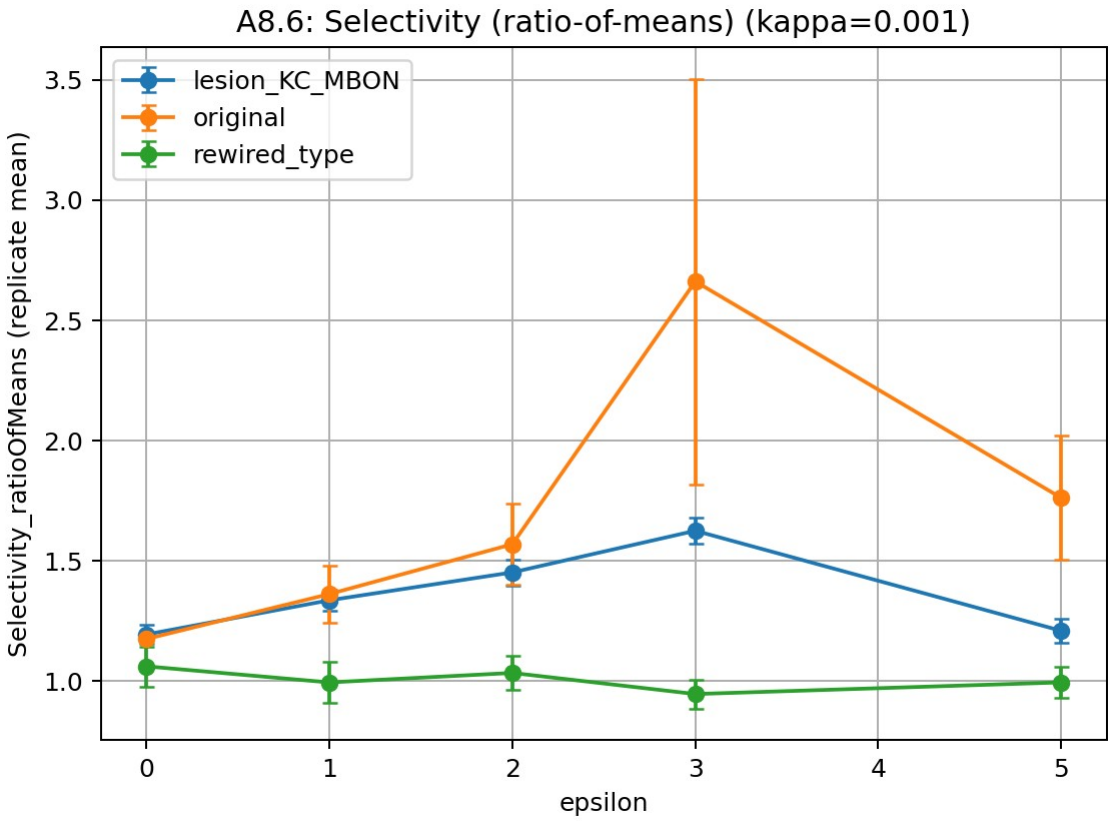

Supplementary Figure S11. Selectivity ratio-of-means vs ε at κ=0.001 (A8.6).

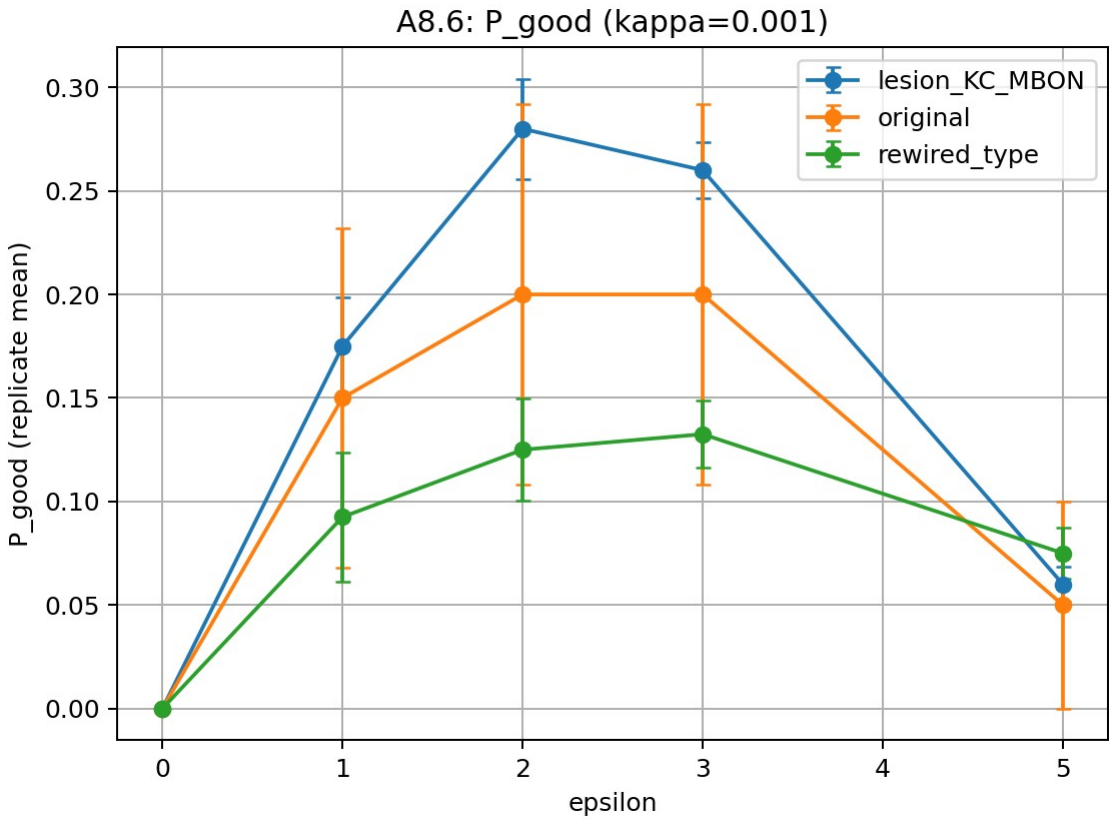

Supplementary Figure S12. P_good vs ε at κ=0.001 (θ=2.0, pT_min=0.005).

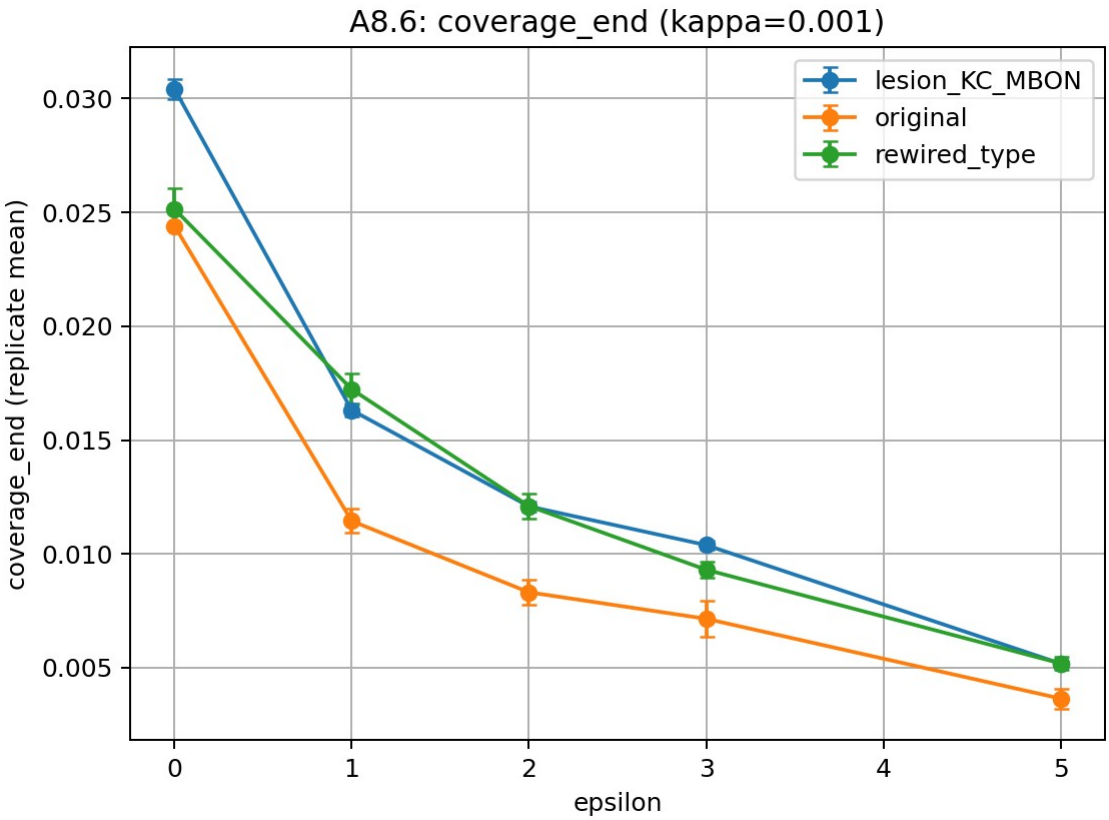

Supplementary Figure S13. coverage_end vs ε at κ=0.001 (A8.6).

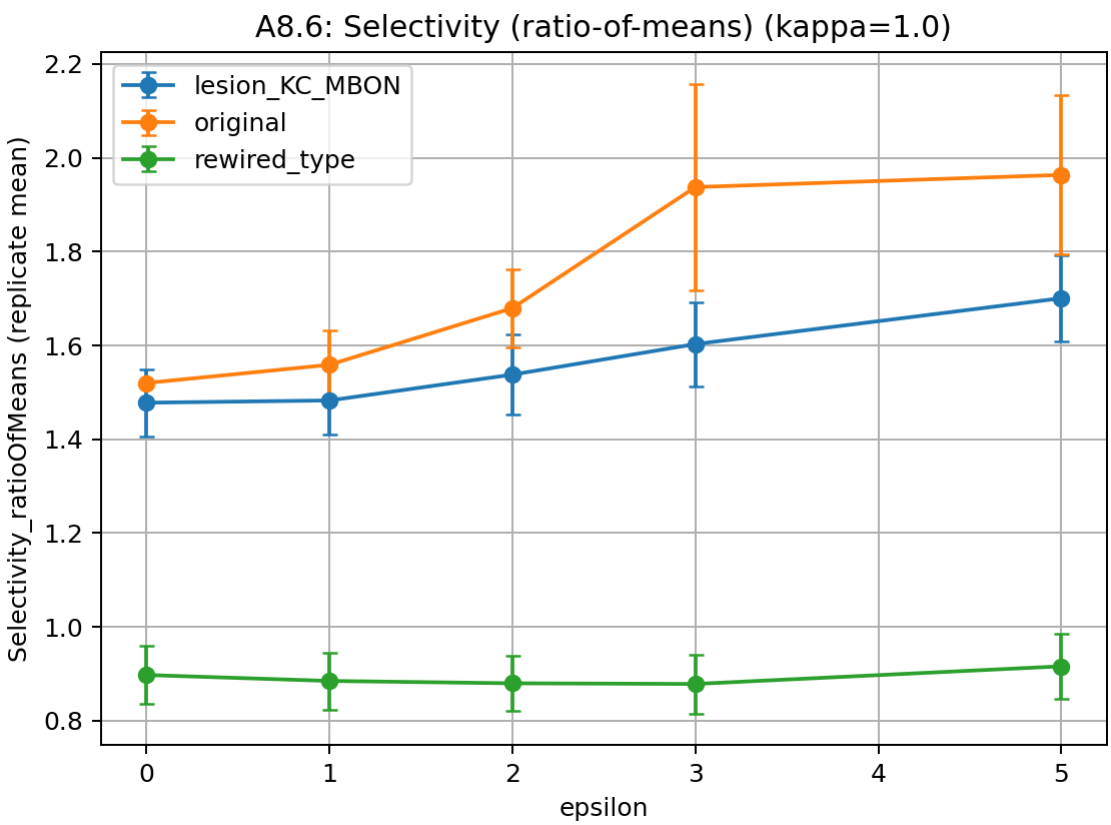

Supplementary Figure S14. Selectivity ratio-of-means vs ε at κ=1.0 (A8.6).

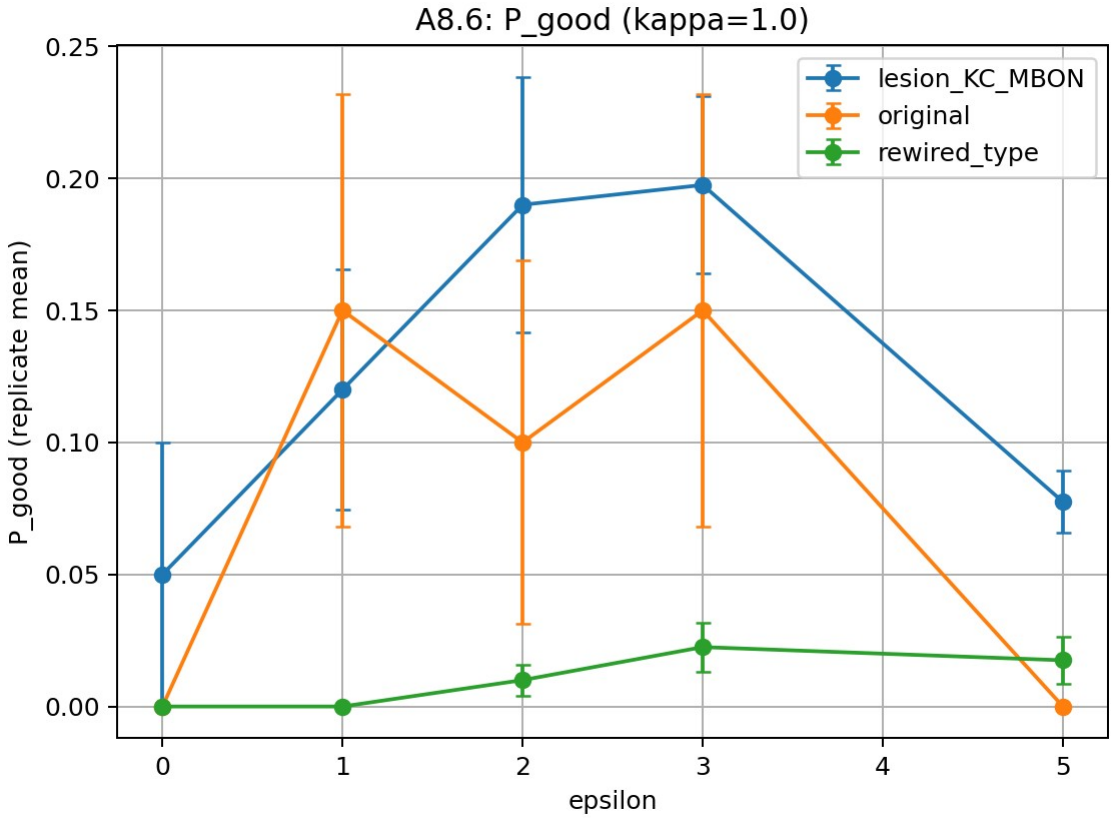

Supplementary Figure S15. P_good vs ε at κ=1.0 (θ=2.0, pT_min=0.005).

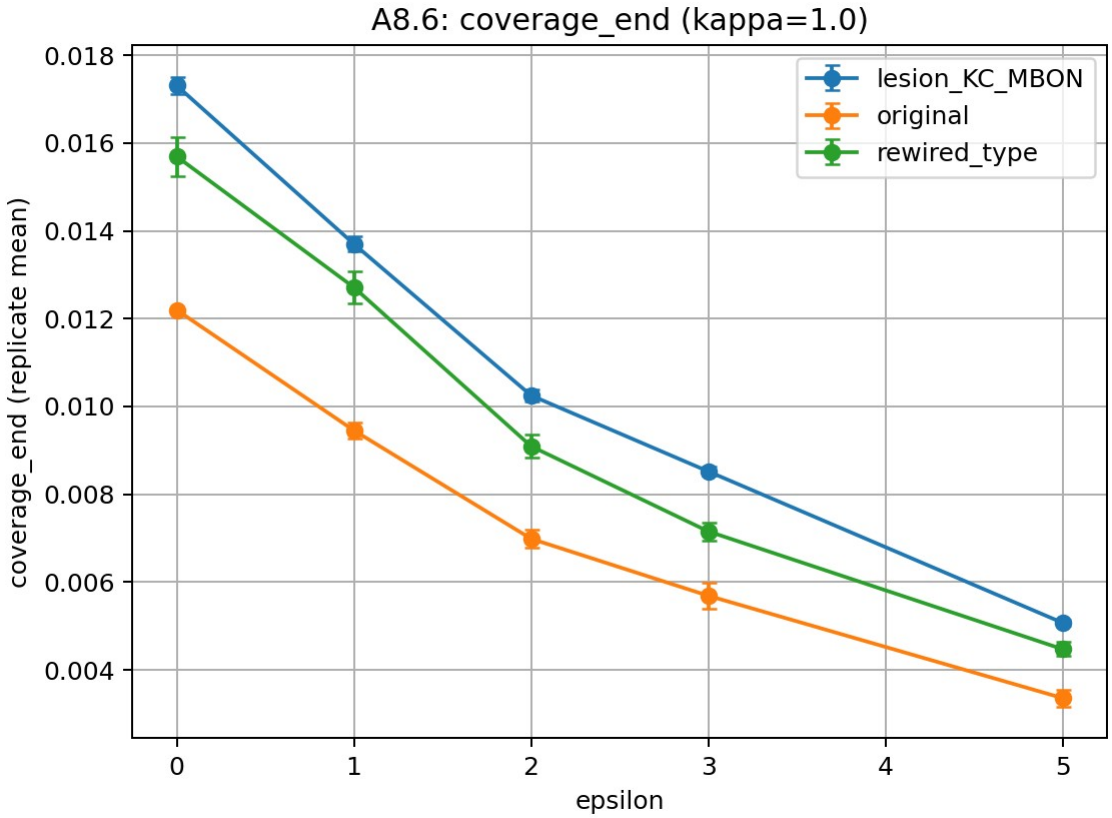

Supplementary Figure S16. coverage_end vs ε at κ=1.0 (A8.6).

S10. Mouse cortical proxy: energy–selectivity trade-off (Steps 2–5)

Summary tables from Steps 2–3 are reproduced below; an additional phase diagram is shown in Figures S17–S18.

Table S9. Cortex proxy transport summary (Step2).

T_env	n	recall_mean	recall_std	recall_ci95	leakage_mean	leakage_std	leakage_ci95	selectivity_ratio_of_means
0.1	100	0.4797	0.2356	0.04619	0.3998	0.2139	0.04193	1.2
1	100	0.2751	0.05368	0.01052	0.6574	0.05673	0.01112	0.4185
inf	100	0.2667	4.898e-15	9.6e-16	0.6667	1.223e-14	2.398e-15	0.4

Table S10. Cortex proxy memory summary (Step3).

T_env	n	recall_mean	recall_ci95	leakage_mean	leakage_ci95	selectivity_ratio_of_means	recall_frac_mean	recall_minus_leakage_mean
0.01	20	0.5674	0.08386	0.2754	0.06837	2.06	0.6787	0.292
0.05	20	0.5644	0.09484	0.2898	0.07687	1.947	0.6597	0.2746

0.1	20	0.4742	0.08977	0.4089	0.09207	1.16	0.543	0.06529
0.2	20	0.3221	0.05987	0.5979	0.07434	0.5387	0.3554	-0.2758
0.5	20	0.2721	0.02415	0.6583	0.02757	0.4133	0.2925	-0.3862
1	20	0.274	0.01684	0.6546	0.01968	0.4186	0.2952	-0.3806
2	20	0.2708	0.009924	0.6589	0.01226	0.4109	0.2913	-0.3881
5	20	0.2678	0.004121	0.6638	0.005326	0.4035	0.2875	-0.3959
10	20	0.2671	0.002057	0.6653	0.002695	0.4014	0.2865	-0.3982
inf	20	0.2667	1.849e-15	0.6667	4.622e-15	0.4	0.2857	-0.4

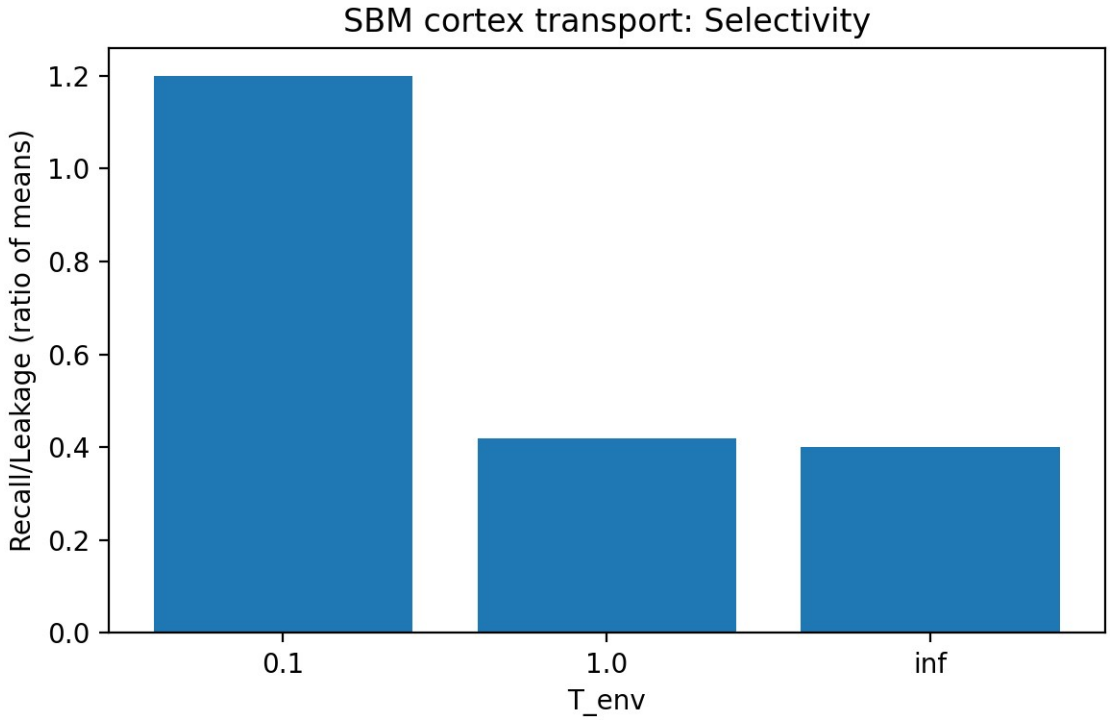

Supplementary Figure S17. Selectivity vs T_env (Step2).

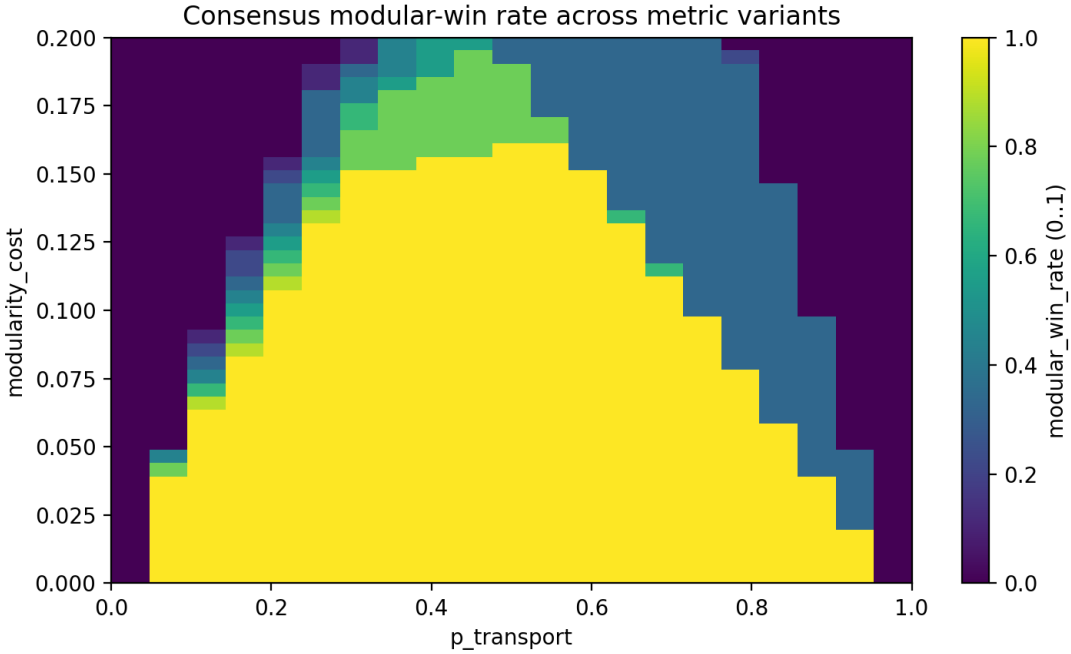

Supplementary Figure S18. Consensus phase diagram in (κ, Δ) space (Step5 robustness audit).

Supplementary References

1. Anderson, P. W. (1958). Absence of diffusion in certain random lattices. Physical Review, 109(5), 1492–1505.

2. Lindblad, G. (1976). On the generators of quantum dynamical semigroups. Communications in Mathematical Physics, 48, 119–130.

3. Gorini, V., Kossakowski, A., & Sudarshan, E. C. G. (1976). Completely positive dynamical semigroups of N-level systems. Journal of Mathematical Physics, 17(5), 821–825.

4. Landauer, R. (1961). Irreversibility and heat generation in the computing process. IBM Journal of Research and Development, 5(3), 183–191.

5. Lennie, P. (2003). The cost of cortical computation. Current Biology, 13(6), 493–497.

6. Friston, K. (2010). The free-energy principle: a unified brain theory? Nature Reviews Neuroscience, 11, 127–138.

7. Hopfield, J. J. (1982). Neural networks and physical systems with emergent collective computational abilities. PNAS, 79(8), 2554–2558.

8. Plenio, M. B., & Huelga, S. F. (2008). Dephasing-assisted transport: quantum networks and biomolecules. New Journal of Physics, 10, 113019.

9. Varshney, L. R., Chen, B. L., Paniagua, E., Hall, D. H., & Chklovskii, D. B. (2011). Structural properties of the Caenorhabditis elegans neuronal network. PLoS Computational Biology, 7(2), e1001066.

10. Winding, M. et al. (2023). The connectome of an insect brain. Science, 379, eadd9330.

11. Yerkes, R. M., & Dodson, J. D. (1908). The relation of strength of stimulus to rapidity of habit-formation. Journal of Comparative Neurology and Psychology, 18, 459–482.

12. Anokhin, K. (2021). Cognitome concept and engram network perspective.